Efficient CsPbBr3 Perovskite Light-Emitting Diodes Enabled by Synergetic Morphology Control

Li-Peng Cheng, Jing-Sheng Huang, Yang Shen, Guo-Peng Li, Xiaoke Liu, Wei Li, Yu-Han Wang, Yan-Qing Li, Yang Jiang, Feng Gao, Chun-Sing Lee and Jian-Xin Tang

Tweet

LIU LINKÖPING UNIVERSITY

Efficient CsPbBr₃ Perovskite Light-Emitting Diodes Enabled by Synergetic Morphology Control

Li-Peng Cheng, Jing-Sheng Huang, Yang Shen, Guo-Peng Li, Xiao-Ke Liu, Wei Li, Yu-Han Wang, Yan-Qing Li,* Yang Jiang, Feng Gao,* Chun-Sing Lee,* and Jian-Xin Tang*

L. P. Cheng, J. S. Huang, Y. Shen, W. Li, Y. H. Wang, Prof. Y. Q. Li, Prof. J. X. Tang
Institute of Functional Nano & Soft Materials (FUNSOM), Jiangsu Key Laboratory for Carbon-Based Functional Materials & Devices, Soochow University, Suzhou 215123, China
E-mail: jxtang@suda.edu.cn (J.X. Tang), yqli@suda.edu.cn (Y.Q. Li)

Dr. G. P. Li, Prof. Y. Jiang
School of Materials Science and Engineering, Hefei University of Technology (HFUT), Hefei, Anhui, 230009, P. R. China

Dr. X. K. Liu, Prof. F. Gao
Biomolecular and Organic Electronics, IFM, Linköping University, 58183 Linköping, Sweden
E-mail: fenga@ifm.liu.se (F. Gao)

Prof. C.-S. Lee
Center of Super-Diamond and Advanced Film (COSADF) and Department of Chemistry, City University of Hong Kong, Hong Kong S.A.R., P.R. China
E-mail: apcslee@cityu.edu.hk

Prof. J. X. Tang
Institute of Organic Optoelectronics (IOO), JITRI, Wujiang, Suzhou, China

The development of solution-processed all-inorganic perovskite light-emitting diodes

(PeLEDs) is currently hindered by low emission efficiency due to morphological defects and

severe non-radiative recombination in all-inorganic perovskite emitter. Herein, bright PeLEDs

are demonstrated by synergetic morphology control over cesium lead bromide (CsPbBr₃)

perovskite films with the combination of two additives. The phenethylammonium bromide

(PEABr) additive enables the formation of mixed-dimensional CsPbBr₃ perovskites featuring

the reduced grain size (<15 nm) and efficient energy funneling, while the dielectric polyethyleneglycol (PEG) additive promotes the formation of highly compact and pinhole-free perovskite films with defect passivation at grain boundaries. Consequently, all-inorganic green PeLEDs achieve a current efficiency of 37.14 cd A^{-1} and an external quantum efficiency of 13.14% with the maximum brightness up to 45990 cd m^{-2} and high color purity. Furthermore, this method can be effectively extended to realize flexible PeLEDs on plastic substrates with a high efficiency of 31.0 cd A^{-1}.

1. Introduction

Solution-processed metal halide perovskite light-emitting diodes (PeLEDs) are attracting great attention for the applications in next-generation optoelectronics due to their high photoluminescence quantum-yield (PLQY), easily tunable bandgap, high color purity, and excellent charge transport properties.[1-10] Since the first report on PeLEDs using organic-inorganic hybrid perovskites (e.g., CH$_3$NH$_3$PbBr$_3$) as the emitter,[1] their external quantum efficiency (EQE) has risen dramatically from initial 0.76% to 14.36% for red and green emissions.[11] Regardless of the rapid progress in PeLEDs,[1,6,11-13] chemical and thermal stabilities of organic-inorganic hybrid perovskites are subject to a debate due to the weak ion binding force between organic cation and metal anion. As a comparison, all-inorganic perovskites like cesium lead bromide (CsPbBr$_3$) hold great promise as an alternative emitter to circumvent the issue on stability.[4,7-10,14-18]

However, device performance of all-inorganic PeLEDs is commonly limited with low brightness and EQE due to the severe current leakage and high non-radiative recombination losses, which are caused by incomplete surface coverage and increased defects at grain boundaries. In the past few years, various approaches have been proposed to enhance the device performance of CsPbBr$_3$-based PeLEDs through morphology control over CsPbBr$_3$ perovskite films or the incorporation of CsPbBr$_3$ quantum-dots.[7-9,14-18] For example, CsBr-

rich precursor solution was usually prepared to reduce defect density without changing the crystal structure of the $CsPbBr_3$ perovskites.[18] Additives were also introduced into perovskite precursor solutions to improve film uniformity and coverage with small grains that can spatially confine exciton diffusion or reduce defect density at the grain boundaries to suppress the photoluminescence (PL) quenching.[6,14] Recently, an efficient $CsPbBr_3$ PeLED has been demonstrated with a peak EQE of 10.4%, in which an organic cation methylammonium bromide (MABr) was incorporated into the $CsPbBr_3$ perovskite.[19]

Despite of the progress abovementioned, the $CsPbBr_3$ perovskite with bulk three-dimensional (3D) crystal structure has small exciton binding energy (~40 meV) and long charge diffusion length,[2] giving rise to low PLQYs at low excitation densities due to the nature of carrier density dependence of bimolecular recombination. To overcome this limitation, an effective strategy is to reduce the grain size in perovskite films to spatially confine the charge carriers for the enhancement of radiative monomolecular (excitonic) recombination.[1,6] In addition, two-dimensional (2D) Ruddlesden-Popper perovskites with layered structures have been developed recently by intercalating large organic counter-cations within the lead halide networks, leading to higher PL efficiency due to enlarged exciton binding energy and concentrated charge carriers.[11,12,20-23] For instance, phenethylammonium bromide (PEABr) has been incorporated to form mixed-dimensional $CsPbBr_3$ perovskites, which can facilitate the radiative recombination along with higher PLQYs and improved device performance in PeLEDs due to efficient energy funneling from larger bandgap (2D) domains to the lowest bandgap (3D) radiative domains.[11,12,20,21] To further optimize the all-inorganic PeLEDs, it is of critical importance to explore an effective strategy for fabricating smooth and pinhole-free $CsPbBr_3$ perovskite films with improved morphological and photophysical properties.

Here, we demonstrate synergetic morphology control over $CsPbBr_3$ perovskite films by incorporating two additives, PEABr and polyethyleneglycol (PEG), to achieve all-inorganic

PeLEDs with high brightness and EQEs. PEABr enables the formation of mixed-dimensional CsPbBr$_3$ perovskites featuring reduced grain size and efficient energy funneling, while PEG promotes the uniformity of perovskite films with higher surface coverage and reduced defect density at grain boundaries. Smooth and pinhole-free CsPbBr$_3$ perovskite films with suppressed current leakage and non-radiative recombination losses are obtained, allowing a substantial increase in both brightness and efficiency of all-inorganic PeLEDs with green emission. The best PeLED yields a current efficiency (CE) of 37.14 cd A^{-1}, an EQE of 13.14%, a maximum luminance of 45,990 cd m^{-2} and high color purity with the full-width at half-maximum (FWHM) of 18 nm. Furthermore, efficient flexible PeLEDs with state-of-the-art performance are realized on plastic substrates, showing a CE of 31.0 cd A^{-1} and an EQE of 10.1%.

2. Results and Discussion

2.1. CsPbBr3 Perovskite Films

Figure 1a presents schematic synthetic procedures of the CsPbBr$_3$ perovskite films with the PEG and PEABr additives (see the details in **Experimental Section**). The transparent CsPbBr$_3$ precursor solutions were prepared by mixing the solution of cesium bromide (CsBr), lead bromide (PbBr$_2$) and PEABr in dimethyl sulfoxide (DMSO) with the PEG solution in different weight ratios (see their chemical structures in Figure 1b). Here, excess CsBr was used in the CsPbBr$_3$ precursor solution to minimize the formation of metallic Pb atoms and thereby suppress the exciton quenching.[18] The molar ratio of CsBr:PbBr$_2$ was optimized to be 1.5:1 in the non-stoichiometric solution which delivers the best device performance in PeLEDs (Table S1). The CsPbBr$_3$ perovskite films were obtained by spin-coating the precursor solution on the indium-tin-oxide (ITO) glass substrates coated with poly(3,4-ethylenedioxythiophene):poly(styrenesulfonate) (PEDOT:PSS), followed by thermal annealing.

Figure 2a displays X-ray diffraction (XRD) patterns of CsPbBr$_3$ perovskite films with/without additive(s). These CsPbBr$_3$ perovskite films are dominated by an orthorhombic (Pnma) crystal structure, consistent with the previous reports.[14,18,24] The characteristic peaks at 15.1°, 21.5°, 30.3°, 35.3°, and 37.6° can be assigned to (101), (121), (202), (141), and (321) crystal planes, respectively. Moreover, the CsPbBr$_3$ perovskite films maintain the identical XRD patterns with the variation of PEABr or PEG content, indicating that the addition of a small amount of PEABr or PEG additive does not significantly affect the intrinsic crystal structure (see Figure S1a).[14,20]

The morphology of the CsPbBr$_3$ perovskite films on PEDOT:PSS-coated substrates was characterized by scanning electron microscopy (SEM). As shown in Figure 2b, pure CsPbBr$_3$ film without any additive shows incomplete surface coverage with discrete large grains (~200 nm), probably leading to severe current leakage and limiting the device performance of PeLEDs. As a comparison, the morphology of the CsPbBr$_3$ perovskite films can be dramatically improved with the addition of PEABr or/and PEG. It is evident in Figure 2b that the PEABr additive enables the growth of small grains in the CsPbBr$_3$ perovskite films (hereafter termed CsPbBr$_3$+PEABr), whereas the CsPbBr$_3$ film with PEG (hereafter termed CsPbBr$_3$+PEG) exhibits compact morphology with high surface coverage and few pinholes. More importantly, PEABr and PEG have synergetic effects on the morphology control over CsPbBr$_3$ perovskites (hereafter termed CsPbBr$_3$+PEG+PEABr), leading to smooth and pinhole-free films with small grains (<15 nm). However, it is worth noting that the weight ratios of PEABr and PEG to CsPbBr$_3$ in the premixed precursor solutions are crucial for the perovskite film growth (Figure S1). For example, a large amount of PEABr (>20%) will result in rough surface of the CsPbBr$_3$ perovskite films owing to the increased hydrophobicity (Figure S1b). The optimal weight ratios of PEABr and PEG to CsPbBr$_3$ are about 10% and 3.8%, respectively, by taking into account the effects of PEABr and PEG contents on film morphology, optical properties and device performance (Figures S1-S5). Under such optimal

conditions, the CsPbBr$_3$+PEG+PEABr perovskite films exhibit a smooth morphology with the highest surface coverage and the most uniform grain sizes (<15 nm).

Figure 2c displays the optical properties of various CsPbBr$_3$ perovskite films on PEDOT:PSS. The typical absorption peak of pure CsPbBr$_3$ appears at around 520 nm (direct bandgap $\approx$ 2.38 eV), while the corresponding PL peak remains at the same position, indicating a low exciton binding energy in the CsPbBr$_3$ perovskite.[20] There is no obvious change in the absorption and PL peak positions in the CsPbBr$_3$+PEG perovskite film (Figure 2c), while its PL intensity is strongly enhanced under the same ultraviolet (UV) illumination (see the photo in Figure 2c). Compared to the CsPbBr$_3$+PEG perovskite film, the addition of PEABr induces blue-shifts of the absorption and PL peaks in either CsPbBr$_3$+PEABr or CsPbBr$_3$+PEG+PEABr perovskite film (Figure 2c). It is evident that increasing PEABr content induces the gradual blue-shift of the absorption and PL peaks in the CsPbBr$_3$+PEG+PEABr perovskite film (Figure S3). More interestingly, when the weight ratio of the PEABr additive in the precursor solution is or exceeds 10%, four additional excitonic absorption peaks can be observed at the short wavelength region and become more apparent along with the attenuation of the bandgap absorption peak at about 510 nm (Figure S3a). According to previous reports,[20,22,24,25] such a phenomenon originates from the formation of layered perovskite structures in the formula of PEA$_2$(CsPbBr$_3$)$_{n-1}$PbBr$_4$, where n is the number of the PbBr$_4^{2-}$ octahedra sheets between two organic PEA insulating layers. Accordingly, n = 1 and n = ∞ correspond to pure 2D (PEA)$_2$PbBr$_4$ phase and bulk 3D CsPbBr$_3$ phase, respectively. With smaller n numbers, quantum confinement effect will be dominant with the increase in the bandgap and exciton energies.[20] Therefore, those four excitonic absorption peaks centered at about 400 nm, 430 nm, 460 nm and 480 nm (Figure S3a) can be assigned to quasi-2D PEA$_2$(CsPbBr$_3$)$_{n-1}$PbBr$_4$ excitonic absorptions with n = 1, 2, 3 and 4, respectively.[20,26] These absorption characteristics imply that the CsPbBr$_3$+PEG+PEABr

perovskites are composed of mixed-dimensional perovskite phases including various quasi-2D $PEA_2(CsPbBr_3)_{n-1}PbBr_4$ structures with different exciton energies.

To understand the carrier dynamics in the $CsPbBr_3$ perovskite films, time-resolved PL decays were recorded at the wavelength of the PL emission peaks (Table S2). Figure 2d plots the PL decay curves, which are fitted with a bi-exponential decay function consisting of a fast-decay component (τ_1) and a slow-decay component (τ_2).[6] Table S2 summarizes the characteristic decay times and the calculated average lifetimes (τ_{avg}). Pure $CsPbBr_3$ perovskite exhibits the shortest PL lifetime of τ_{avg} = 12.07 ns. Notably, the addition of PEABr or PEG prolongs the PL lifetime of the perovskite films, suggesting that these two additives can passivate the defects at grain boundaries and suppress the defect-assisted non-radiative recombination. More importantly, the $CsPbBr_3$+PEG+PEABr perovskite has the longest lifetime of τ_{avg} = 62.44 ns (Table S2). This means that PEABr and PEG have the synergetic effects on morphology control as well as defect passivation. As discussed above and shown in Figure S3, the addition of PEABr leads to the formation of mixed-dimensional perovskite phases, where energy funneling may occur from the larger 2D bandgap to the lower bulk 3D bandgap domains. To verify this viewpoint, the PL decay characteristics of the perovskite films at various emission wavelengths were further detected under the excitation of 370 nm laser pulses (Figure S6). As compared to the cases of pure $CsPbPb_3$ and $CsPbPb_3$+PEG films, the time-resolved PL decay curves (at 520 nm) of the $CsPbPb_3$+PEABr and $CsPbPb_3$+PEG+PEABr perovskite films exhibit clear rise times of 1-2 ns. However, such differences cannot be observed for the PL decays at other emission wavelengths (e.g., 420 nm and 460 nm). This observation indicates that the filling time of excited states, of which the energy corresponds to the emission wavelength of 520 nm, is quite slower in either the $CsPbPb_3$+PEABr or the $CsPbPb_3$+PEG+PEABr perovskite film, suggesting that the excited state population in these two films primarily results from energy transfer happening within 1-

2 ns after laser pulse-induced direct excitation. Such observations are consistent with the previous works which demonstrated that efficient energy transfer from the larger 2D bandgap to the lower bulk 3D bandgap domains can enhance the radiative recombination.[11,12]

2.2. Formation Mechanism

Figure 3 illustrates the mechanisms of the morphology control over $CsPbBr_3$ perovskite films with PEG and PEABr additives. During the volatilization of the DSMO solvent in the spin-coating process, the $CsPbBr_3$ perovskite is continuously crystallized from the precursor solution with ionic interactions between metal cations and halogen anions. As the residual DMSO solvent dries slowly in the perovskite layer, the $CsPbBr_3$ perovskite usually grows into large grains, resulting in the incomplete surface coverage with numerous pinholes (Figure 3a). The PEABr additive can dramatically impede the continuous growth of $CsPbBr_3$ perovskites by intercalating at the grain boundaries to restrain their bonding interaction (Figure 3b). During this process, partial replacement of Cs^+ ions with PEA^+ at the grain boundaries will take place and thus limit the grain growth of bulk 3D perovskite structure in one dimension, leading to the formation of 2D perovskite crystals in the formula of $PEA_2(CsPbBr_3)_{n-1}PbBr_4$ with small grains. Similar to previous reports,[11,12] such a mixed-dimensional perovskite film is composed of a mixture of various n-phases. The bandgap of mixed-dimensional $CsPbBr_3$ perovskite films will increase gradually with a continuous increase in PEABr content, leading to a blue-shift of the emission peak from 520 nm to 507 nm (Figure S3). Although the mixed-dimensional perovskite structure has good stability, its surface roughness is relatively large that limits the device performance. PEG with good solubility and rheology is a kind of Lewis base that can bind with Lewis acid Pb^{2+}.[27] Therefore, the addition of a small amount of PEG can limit the diffusion of the $CsPbBr_3$ precursors through chemical interactions (Figure 3c). The improved morphology with low surface roughness and low pinhole densities in the perovskite films (Figure 2b) is thus realized since the PEG additive can promote the uniformity of the perovskite films as a matrix to fill the grain boundaries and passivate the

8

defects at the grain surface due to the defect healing effect. Accordingly, the combination of PEG and PEABr additives can induce the synergetic effect on the morphology control over mixed-dimensional $CsPbBr_3$ perovskite films with the reduced grain size and the passivation of defect density at the grain boundaries (Figure 3d). As compared with pure $CsPbBr_3$ perovskite films, the suppression of current leakage and non-radiative recombination rate can be expected in the $CsPbBr_3$+PEG+PEABr perovskite film because of the PL enhancement and the prolonged emission lifetime (Figure 2).

2.3. Device Performance

The PeLEDs are constructed using different $CsPbBr_3$ perovskite films with the same device architecture of glass/ITO/PEDOT:PSS/ $CsPbBr_3$ perovskite/TPBi/LiF/Al, where ITO is used as an anode, PEDOT:PSS as a hole-transport layer (HTL), $CsPbBr_3$ perovskite as an emitting layer, 2,2',2"-(1,3,5-Benzinetriyl)- tris(1-phenyl-1-H-benzimidazole) (TPBi) as an electron-transport/hole-blocking layer (ETL/HBL), and LiF/Al as a bilayer cathode (see the details in **Experimental Section**). **Figure 4**a shows the energy level diagram of the PeLED, in which the energy level positions of all function layers refer to the previous reports.[11,13,14] It is expected that holes can be effectively confined for the exciton formation in the $CsPbBr_3$ perovskite films due to the deep highest occupied molecular orbital (HOMO) level of TPBi. The device characteristics of various PeLEDs are plotted in Figure 4b-4g, and the detailed device performances are summarized in **Table 1**. The PeLED with pure $CsPbBr_3$ exhibits a maximum luminance of 9,662 cd m^{-2}, while the CE and EQE are limited to 2.5 cd A^{-1} and 0.76%, respectively. Such poor performance may be ascribed to the large current leakage and high non-radiative recombination resulting from poor film morphology with numerous pinholes and defects at the grain boundaries. It is obvious in Figure 4b that the addition of PEG or PEABr in the $CsPbBr_3$ perovskite films induces lower current density as compared to that of pure $CsPbBr_3$ under the same bias voltage, while a substantial increase in luminance and efficiency is achieved for PeLEDs using $CsPbBr_3$ perovskite films with PEG or PEABr

9

additive (Figure 4b-4d). For example, the PeLED with $CsPbBr_3$+PEG perovskite film exhibits the enhanced CE and EQE up to 5.05 cd A^{-1} and 1.39%, respectively. As suggested by the SEM and PL decay results, such an efficiency improvement is attributed to the compact and pinhole-free morphology of the $CsPbBr_3$+PEG perovskite film and the reduced non-radiative recombination. The injection-current of PeLEDs with $CsPbBr_3$+PEABr perovskite film is to some extent lower than that using pure $CsPbBr_3$ or $CsPbBr_3$+PEG perovskite film, which is mainly correlated to the limited charge transport properties of mixed-dimensional $CsPbBr_3$ structure with small grain size and incomplete surface coverage. However, the remarkable enhancement in CE and EQE of the $CsPbBr_3$+PEABr-based device indicates the increase in radiative recombination efficiency due to the presence of mixed-dimensional perovskite structure for more efficiently exciton generation as demonstrated in the PL measurement (Figure 2). Correspondingly, the combination of PEG and PEABr causes the synergetic effect on morphology control over $CsPbBr_3$ perovskite films with high surface coverage, which can suppress the current leakage and possibly improve the electron-hole balance for the increased radiative recombination efficiency. As a result, the PeLED using $CsPbBr_3$+PEG+PEABr perovskite film as the emitter outperforms the device with pure $CsPbBr_3$ by an order of magnitude in both luminance and efficiency. For instance, a maximum luminance of 45,990 cd m^{-2} is obtained for the $CsPbBr_3$+PEG+PEABr-based PeLED along with a maximum CE of 37.14 cd A^{-1} and a maximum EQE of 13.14%, respectively, which are 17 times that of the device with pure $CsPbBr_3$ (Table 1). More remarkably, the device shows small efficiency roll-off at high luminance. The EQE of the $CsPbBr_3$+PEG+PEABr-based device remains at a high value of 9.3% along with a CE of 31.2 cd A^{-1} even at a high luminance of 10,000 cd m^{-2}. In addition, the EQE histogram displayed in Figure 4e reveals high reproducibility of the $CsPbBr_3$+PEG+PEABr-based PeLED. The variation of the device performance of PeLEDs with different perovskite films can be correlated to the film quality, which is consistent with the comparison of morphological and optical properties among $CsPbBr_3$ perovskites with

different PEG and PEABr contents (Figures S4-S5 and Table S3). The normalized electroluminescence (EL) spectra of the PeLEDs in Figure 4f exhibit single green emission centered at the same wavelengths as the PL peaks (Table 1), and the EL spectra are stable under various bias voltages (Figure S7). Stable and clean EL emission can be obtained under continuous operation of the devices (inset in Figure 4f). In addition, the EL spectra show excellent color purity (85%) in the green region with a narrow FWHM of ~18 nm. The corresponding Commission Internationale de I'Eclairage (CIE) chromaticity coordinates (x, y) of the $CsPbBr_3$+PEG+PEABr-based PeLEDs are (0.092, 0.753) (Figure 4g). These results demonstrate that the performance enhancement of $CsPbBr_3$ PeLEDs is primarily attributed to the synergetic interplay of PEG and PEABr additives on the morphology optimization which results in a smooth and pinhole-free mixed-dimensional perovskite film, enabling the drastic boost in radiative recombination efficiency due to the efficient energy funneling and spatial carrier confinement in the lowest bandgap 3D phase.

For bendable display and curved lighting applications with PeLEDs, it is highly desirable to realize the flexible device architecture on plastic substrates. However, the efficiency values of flexible PeLEDs reported so far lag behind those of the counterparts on rigid glass substrates.[28-31] To validate the effectiveness of the method in this work, flexible PeLEDs using the $CsPbBr_3$+PEG+PEABr perovskite film were further fabricated on polyethylene terephthalate (PET) substrates, in which Ag nanowires (AgNWs) was used as the transparent electrode to replace the conventional ITO.[32-34] As shown in **Figure 5**a, the AgNWs with a diameter of ~40 nm and a length of 20-30 μm were spin-cast on PET substrates to form a transparent electrode, which possess an optical transmittance of >80% in the visible wavelength region and a sheet resistance of <25 Ω sq^{-1}. The root-mean-square (RMS) roughness of the AgNWs electrode was determined to be ~20 nm (Figure S8a). To smooth the electrode surface, a thicker PEDOT:PSS layer with a thickness of 45 nm was spin-coated on the AgNWs-coated PET substrate, resulting in a RMS roughness of ~6 nm. The morphology

of the CsPbBr$_3$+PEG+PEABr perovskite film grown on flexible PET substrates was measured (Figure 5, Figure S8b), which is almost identical to that on glass substrates. It is noteworthy that flexible PeLED with CsPbBr$_3$+PEG+PEABr perovskite film exhibits a high performance with a maximum EQE of 10.1% and a maximum CE of 31.0 cd A^{-1} (Figure 5c), respectively, which are comparable to the glass-based counterparts. These results indicate that the proposed formation method of the CsPbBr$_3$+PEG+PEABr perovskite film can be effectively used on plastic substrates to obtain high-performance flexible devices.

3. Conclusions

In summary, bright all-inorganic PeLEDs with high EQEs have been demonstrated by synergetic morphology control over CsPbBr$_3$ perovskite films with the combination of PEABr and PEG additives. The PEABr additive enables the formation of mixed-dimensional CsPbBr$_3$ perovskites with small grain size that feature efficient energy funneling, whereas the dielectric PEG additive promotes the morphological uniformity of the perovskite films as a matrix to fill the grain boundaries and passivate the grain surface with reduced defect density. The improved morphology with pinhole-free surface coverage can significantly suppress the current leakage and non-radiative recombination in the resulting perovskite film. Substantial increase in both brightness and efficiency has been achieved in all-inorganic green PeLEDs, among which the best device yields a current efficiency of 37.14 cd A^{-1}, an EQE of 13.14%, a maximum luminance of 45,990 cd m^{-2} and high color purity. To the best of our knowledge, the maximum EQE of our devices is among the highest efficiencies for all-inorganic CsPbBr$_3$-based PeLEDs reported so far (Table S4). Furthermore, efficient flexible PeLEDs with state-of-the-art performance were realized on plastic substrates, showing a CE of 31.0 cd A^{-1} and an EQE of 10.1%. We anticipate that this approach may provide a facile route to improving the halide perovskite-based devices with desirable morphological, optical and electrical properties.

4. Experimental Section

Perovskite Preparation: CsBr and PbBr$_2$ were purchased from TCI (99.0%). PEG (average Mv ~600000), dimethyl sulfoxide (DMSO) (99.7%) and LiF (99.99%) were purchased from MACKLIN. TPBi (99.0%) was purchased from Nichem. PEABr (99.5%) was purchased from Xi'an Polymer. PEDOT:PSS (Clevios P VP Al 4083) was purchased from Heraeus. All the materials were used directly without any treatment. The synthetic procedure of the CsPbBr$_3$ perovskite films with PEG and PEABr additives is shown in Figure 1a. Firstly, the CsPbBr$_3$ precursor solution was prepared by simultaneously dissolving CsBr (60 mg mL^{-1}), PbBr$_2$ (70 mg mL^{-1}), and PEABr (13 mg mL^{-1}) in DMSO. Then, the PEG (10 mg mL^{-1}) in DMSO was mixed with the CsPbBr$_3$ solution to obtain a transparent precursor solution, which was stirred for a few hours at room temperature. Finally, the CsPbBr$_3$ perovskite films were obtained by spin-coating the precursor solution at 3000 rpm for 60 s in a nitrogen-filled glovebox, and subsequently annealed on a hot plate at 70 °C for 5 min to remove the DMSO residual.

Device Fabrication: The PeLEDs were constructed with a structure of glass/ITO/PEDOT:PSS/CsPbBr$_3$ perovskite/TPBi/LiF/Al, in which ITO with a sheet resistance of ~10 Ω sq^{-1} was used as anode, PEDOT:PSS as hole-transport layer, CsPbBr$_3$ perovskite layer as the green emitter, TPBi as electron-transport layer, and LiF/Al as a bilayer cathode, respectively. ITO-coated glass substrates were cleaned by ultrasonication in detergent, acetone, ethanol, and deionized water for 30 min in sequence, and subsequently dried in an oven (110 °C). Prior to the layer deposition, ITO-coated glass substrates were treated by UV ozone for 15 min. The filtered PEDOT:PSS solution with 0.45 μm poly(tetrafluoroethylene) syringe filters was spin-coated on ITO glass substrates at 4000 rpm for 40 s, and annealed at 140 °C for 15 min in ambient air to form a 40 nm-thick film. The samples were then transferred into a N$_2$-filled glovebox and spin-coated with various CsPbBr$_3$ precursor solutions. Finally, the samples with CsPbBr$_3$ perovskite films were transferred from the N$_2$-filled glovebox into an interconnected high-vacuum deposition system (base pressure

$\approx 5 \times 10^{-7}$ Torr) for thermal evaporation of TPBi (40 nm) and LiF (1 nm)/Al (100 nm) through shadow masks to complete the device. The deposition rate and film thickness were monitored with a quartz crystal oscillator. The effective area of PeLEDs was determined to be 10 mm^2 with the overlap between ITO and Al electrodes. The encapsulation of PeLEDs was carried out with glass lid and epoxy resin. To get consistent results, devices with different perovskite films were usually fabricated in the same batch.

Characterization: The morphologies of CsPbBr$_3$ perovskite films were characterized by field-emission scanning electron microscopy (SEM) (Zeiss Supra 55). XRD patterns were recorded with a Rigaku D/MaxrB diffraction with Cu Kα radiation to characterized the crystal structures of the perovskite films. The ultraviolet-visible absorption spectra were measured with a UV/vis/near-IR spectrophotometer (Perkin Elmer Lambda 750). Steady-state PL spectra and time-resolved PL decays were collected with FluoroMax-4 fluorescence spectrometer (Horiba Jobin Yvon) and Horib-FM-2015 spectrometer, respectively. Current density-voltage-luminance (I-V-L) characteristics and electroluminescence (EL) spectra of PeLEDs were measured simultaneously with a computer-controlled programmable power source (Keithley model 2400) and a luminance meter/spectrometer (PhotoResearch PR655). The EQEs were calculated by taking a full account of the measured I-V-L characteristics and EL spectra of PeLEDs with a Lambertian profile. All the measurements were carried out under ambient conditions at room temperature.

Supporting Information

Supporting Information is available from the Wiley Online Library or from the author.

Acknowledgements

References

[1] Z.-K. Tan, R. S. Moghaddam, M. L. Lai, P. Docampo, R. Higler, F. Deschler, M. Price, A. Sadhanala, L. M. Pazos, D. Credgington, F. Hanusch, T. Bein, H. J. Snaith, R. H. Friend, *Nat. Nanotechnol.* **2014**, *9*, 687-692.

[2] L. Protesescu, S. Yakunin, M. I. Bodnarchuk, F. Krieg, R. Caputo, C. H. Hendon, R. X. Yang, A. Walsh, M. V. Kovalenko, *Nano Lett*. **2015**, *15*, 3692-3696.

[3] G. Xing, N. Mathews, S.S. Lim, N. Yantara, X. Liu, D. Sabba, M. Grätzel, S. Mhaisalkar, T. C. Sum, *Nat. Mater*. **2014**, *13*, 476-480.

[4] J. Song, J. Li, X. Li, L. Xu, Y. Dong, H. Zeng, *Adv. Mater*. **2015**, *27*, 7162-7167.

[5] M. Kulbak, D. Cahen, G. Hodes, *J. Phys. Chem. Lett*. **2015**, *6*, 2452-2456.

[6] H. Cho, S.-H. Jeong, M.-H. Park, Y.-H. Kim, C. Wolf, C.-L. Lee, J. H. Heo, A. Sadhanala, N. Myoung, S. Yoo, S. H. Im, R. H. Friend, T.-W. Lee, *Science* **2015**, *350*, 1222-1225.

[7] X. Li, Y. Wu, S. Zhang, B. Cai, Y. Gu, J. Song, H. Zeng, *Adv. Funct. Mater*. **2016**, *26*, 2435-2445.

[8] X. Zhang, B. Xu, J. Zhang, Y. Gao, Y. Zheng, K. Wang, X. W. Sun, *Adv. Funct. Mater*. **2016**, *26*, 4595-4600.

[9] Y. Ling, Z. Yuan, Y. Tian, X. Wang, J. C. Wang, Y. Xin, K. Hanson, B. Ma, H. Gao, *Adv. Mater.* **2016**, *28*, 305-311.

[10] J. Li, L. Xu, T. Wang, J. Song, J. Chen, J. Xue, Y. Dong, B. Cai, Q. Shan, B. Han, H. Zeng, *Adv. Mater*. **2017**, *29*, 1603885.

[11] X. L. Yang, X. W. Zhang, J. X. Deng, Z. M. Chu, Q. Jiang, J. H. Meng, P. Y. Wang, L. Q. Zhang, Z. G. Yin, J. B. You, *Nat. Commun*. **2018**, *9*, 570.

[12] N. Wang, L. Cheng, R. Ge, S. Zhang, Y. Miao, W. Zou, C. Yi, Y. Sun, Y. Cao, R. Yang, Y. Wei, Q. Guo, Y. Ke, M. Yu1 Y. Jin, Y. Liu, Q. Ding, D. Di, L. Yang, G. Xing, H. Tian, C. Jin, F. Gao, R. H. Friend, J. Wang, W. Huang, *Nat. Photon.* **2016**, *10*, 699-704.

[13] Z. G. Xiao, R. A. Kerner, L. F. Zhao, N. L. Tran, K. M. Lee, T.-W. Koh, G. D. Scholes, B. P. Rand, *Nat. Photon*. **2017**, *11*, 108-115.

[14] Y. Ling, Y. Tian, X. Wang, J. C. Wang J. M. Knox, F. Perez-Orive, Y. Du, L. Tan, K. Hanson, B. Ma, H. Gao, *Adv. Mater*. **2016**, *28*, 8983-8989.

[15] G. Li, F. W. R. Rivarola, N. J. L. K. Davis, S. Bai, T. C. Jellicoe, F. de la Peña, S. Hou, C. Ducati, F. Gao, R. H. Friend, N. C. Greenham, Z.-K. Tan, *Adv. Mater.* **2016**, *28*, 3528-3534.

[16] X. Zhang, H. Lin, H. Huang, C. Reckmeier, Y. Zhang, W. C. H. Choy, A. L. Rogach, *Nano Lett.* **2016**, *16*, 1415-1420.

[17] R. E. Beal, D. J. Slotcavage, T. Leijtens, A. R. Bowring, R. A. Belisle, W. H. Nguyen, G. F. Burkhard, E. T. Hoke, M. D. McGehee, *J. Phys. Chem. Lett.* **2016**, *7*, 746-751.

[18] N. Yantara, S. Bhaumik, F. Yan, D. Sabba, H. A. Dewi, N. Mathews, P. P. Boix, H. V. Demir, S. Mhaisalkar, *J. Phys. Chem. Lett*. **2015**, *6*, 4360−4364.

[19] L. Zhang, X. Yang, Q. Jiang, P. Wang, Z. Yin, X. Zhang, H. Tan, Y. Yang, M. Wei, B. R. Sutherland, E. H. Sargent, J. You, *Nat. Commun*. **2017**, *8*, 15640.

[20] Y. F. Ng, S. A. Kulkarni, S. Parida, N. F. Jamaludin, N. Yantara, A. Bruno, C. Soci, S. Mhaisalkar, N. Mathews, *Chem. Commun.* 2017, 53, 12004-12007.

[21] M. Yuan, L. N. Quan, R. Comin, G. Walters, R. Sabatini, O. Voznyy, S. Hoogland, Y. Zhao, E. M. Beauregard, P. Kanjanaboos, Z. Lu, D. H. Kim and E. H. Sargent, *Nat. Nano*. **2016**, *11*, 872-877.

[22] J. Byun, H. Cho, C. Wolf, M. Jang, A. Sadhanala, R. H. Friend, H. Yang and T.-W. Lee, *Adv. Mater*. **2016**, *28*, 7515-7520.

[23] L. N. Quan, Y. Zhao, F. P. García de Arquer, R. Sabatini, G. Walters, O. Voznyy, R. Comin, Y. Li, J. Z. Fan, H. Tan, J. Pan, M. Yuan, O. M. Bakr, Z. Lu, D. H. Kim, E. H. Sargent, *Nano Lett*. **2017**, *17*, 3701-3709.

[24] M. Kulbak, D. Cahen, G. Hodes, *J. Phys. Chem. Lett.* **2015**, *6*, 2452-2456.

[25] D. Liang, Y. Peng, Y. Fu, M. J. Shearer, J. Zhang, J. Zhai, Y. Zhang, R. J. Hamers, T. L. Andrew, S. Jin, *ACS Nano* **2016**, *10*, 6897-6904.

[26] L. N. Quan, M. Yuan, R. Comin, O. Voznyy, E. M. Beauregard, S. Hoogland, A. Buin, A. R. Kirmani, K. Zhao, A. Amassian, D. H. Kim, E. H. Sargent, *J. Am. Chem. Soc*. **2016**, *138*, 2649-2655.

[27] L. Song, X. Y. Guo, Y. S. Hu, Y. Lv, J. Lin, Z. Q. Liu, Y. Fan, X. Y. Liu, *J. Phys. Chem. Lett*. **2017**, *8*, 4148-4154.

[28] S. G. R. Bade, J. Li, X. Shan, Y. Ling, Y. Tian, T. Dilbeck, T. Besara, T. Geske, H. Gao, B. Ma, K. Hanson, T. Siegrist, C. Xu, Z. Yu, *ACS Nano* **2016**, *10*, 1795-1801.

[29] S. G. R. Bade, X. Shan, P. T. Hoang, J. Li, T. Geske, L. Cai, Q. Pei, C. Wang, Z. Yu, *Adv. Mater.* **2017**, *29*, 1607053.

[30] H.-K. Seo, H. Kim, J. Lee, M.-H. Park, S.-H. Jeong, Y.-H. Kim, S.-J. Kwon, T.-H. Han, S. Yoo, T.-W. Lee, *Adv. Mater.* **2017**, *29*, 1605587.

[31] G. Li, Z.-K. Tan, D. Di, M. L. Lai, L. Jiang, J. H.-W. Lim, R. H. Friend, N. C. Greenham, *Nano Lett*. **2015**, *15*, 2640-2644.

[32] J. Liang, L. Li, X. Niu, Z. Yu, Q. Pei, *Nat. Photon*. **2013**, *7*, 817-824.

[33] T. Sannicolo, M. Lagrange, A. Cabos, C. Celle, J. P. Simonato, D. Bellet, *Small* **2016**, *12*, 6052-6075.

[34] D. Kim, Y. Fu, S. Kim, W. Lee, K.-H. Lee, H. K. Chung, H.-J. Lee, H. Yang, H. Chae, *ACS Nano* **2017**, *11*, 1982-1990.
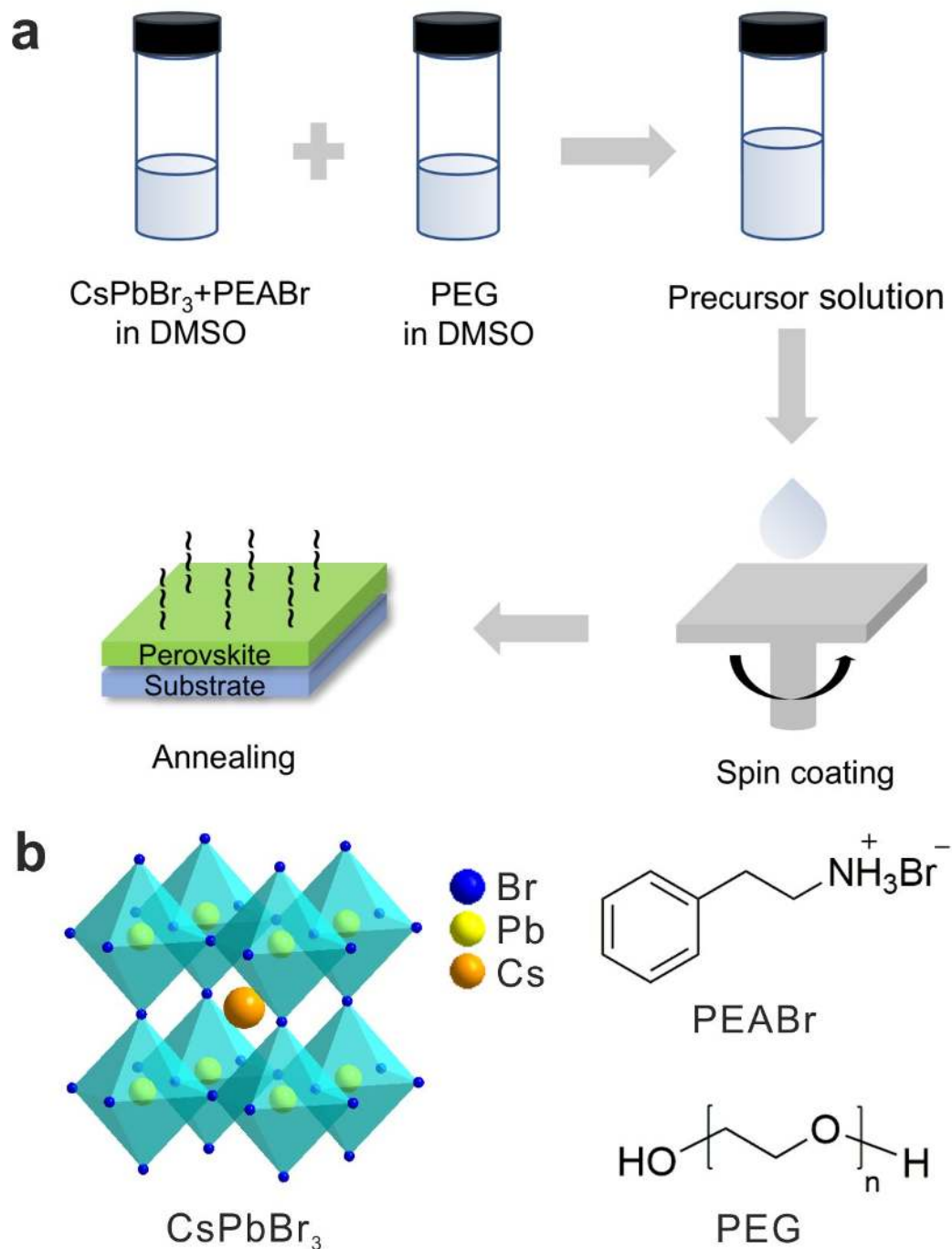
Figure 1. Synthesis of CsPbBr₃-based perovskite thin films. (a) Schematic of the facile solution-based fabrication procedure of the perovskite film with PEABr and PEG additives. (b) Chemical structures of CsPbBr₃, PEABr and PEG.
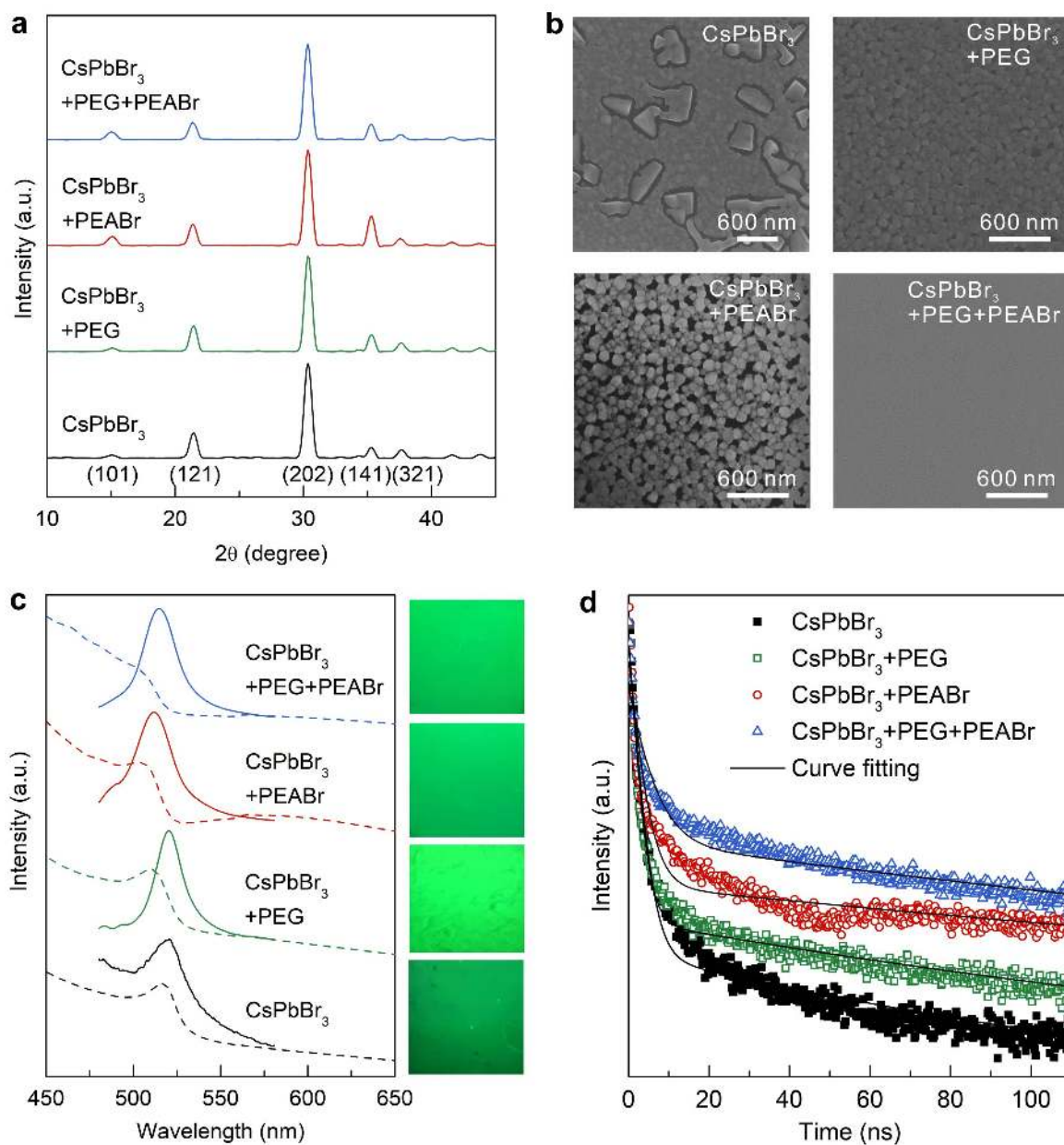
Figure 2. Properties of CsPbBr$_3$ perovskite films. (a) XRD patterns of various CsPbBr$_3$ perovskite films on PEDOT:PSS-coated ITO-glass substrates. (b) SEM images of CsPbBr$_3$ perovskite films with different additives. (c) Absorption (dashed line) and PL (solid line) spectra of CsPbBr$_3$ perovskite thin films on quartz substrates. Inserts: PL images of the CsPbBr$_3$ perovskite films under ultraviolet lamp excitation (Hg lamp, 365 nm). (d) Time-resolved PL decay curves of CsPbBr$_3$ perovskite films measured under the excitation of 370 nm.
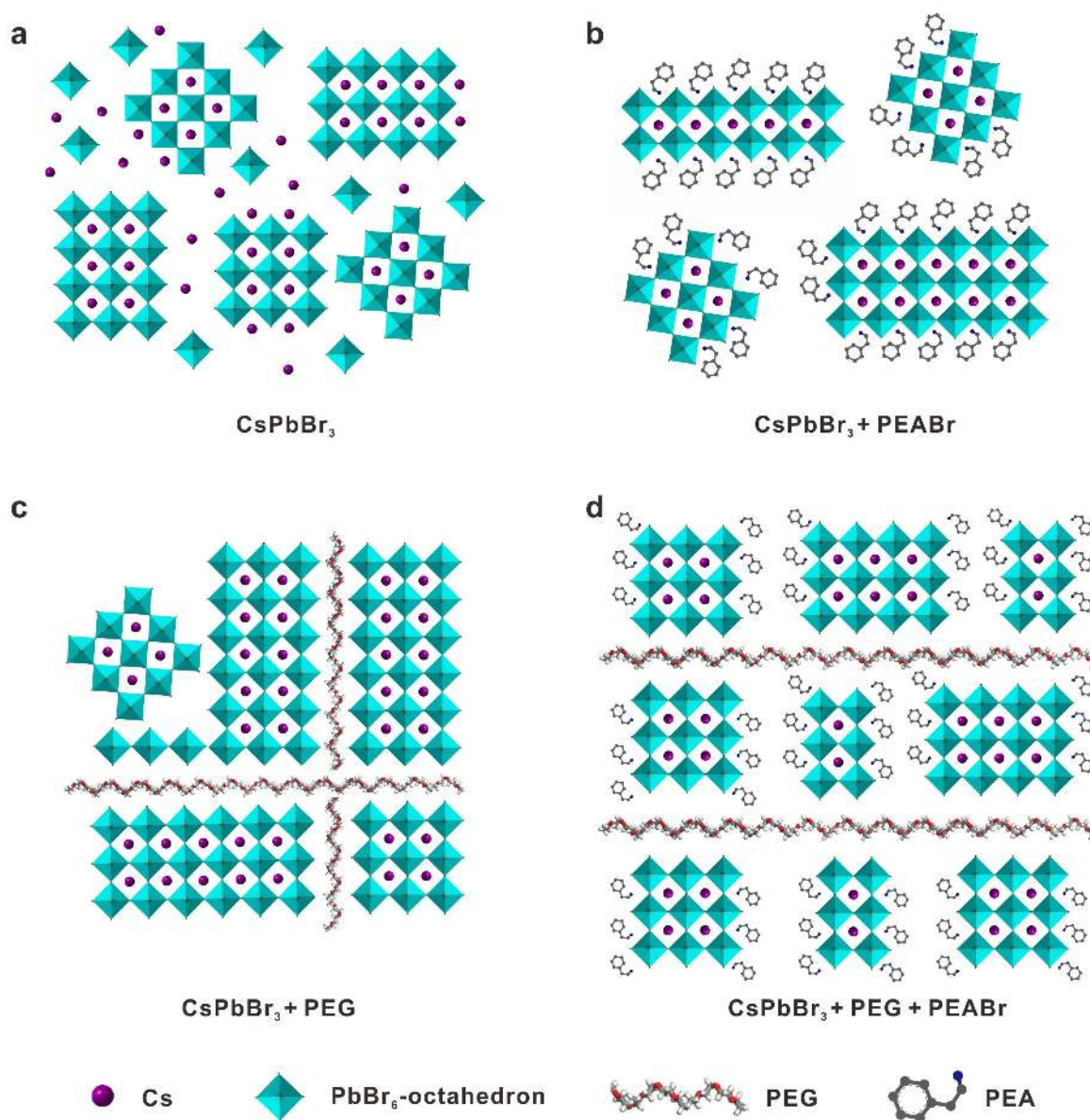
Figure 3. Schematic mechanism of the CsPbBr$_3$ morphology control with the additives. (a) Pure CsPbBr$_3$ without any additive. (b) CsPbBr$_3$ with PEABr. (c) CsPbBr$_3$ with PEG. (d) CsPbBr$_3$ with both PEG and PEABr.
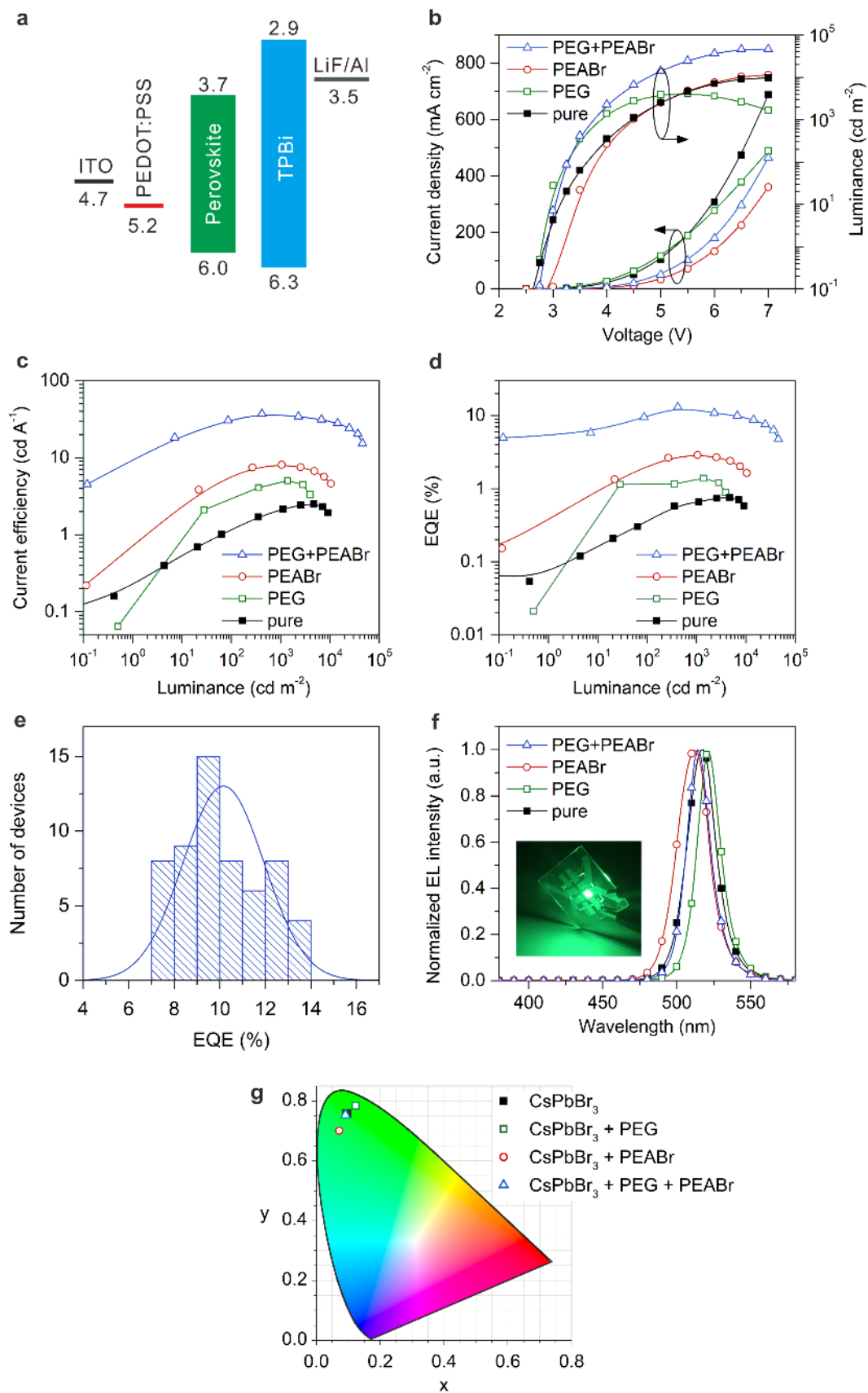
Figure 4. Device structure and performance of CsPbBr₃ PeLEDs. (a) Energy level diagram of

a CsPbBr₃ PeLED consisting of ITO/PEDOT:PSS (40 nm)/CsPbBr₃ (50 nm)/TPBi (40

nm)/LiF (1 nm)/Al (100 nm) (unit: eV). (b) Current density-voltage (I-V) and luminance-voltage (L-V) characteristics. (c) Current efficiency as a function of luminance. (d) EQE as a function of luminance. (e) Histogram of peak EQEs measured from the CsPbBr$_3$+PEG+PEABr-based PeLEDs, which shows an average EQE of 10.3% with a relative standard deviation of 17.5%. (f) EL spectra of various devices working at 4.5 V. Inset: photograph of a device with both PEABr and PEG. (g) The Commission Internationale de I'Eclairage (CIE) coordinates of various CsPbBr$_3$ PeLEDs.
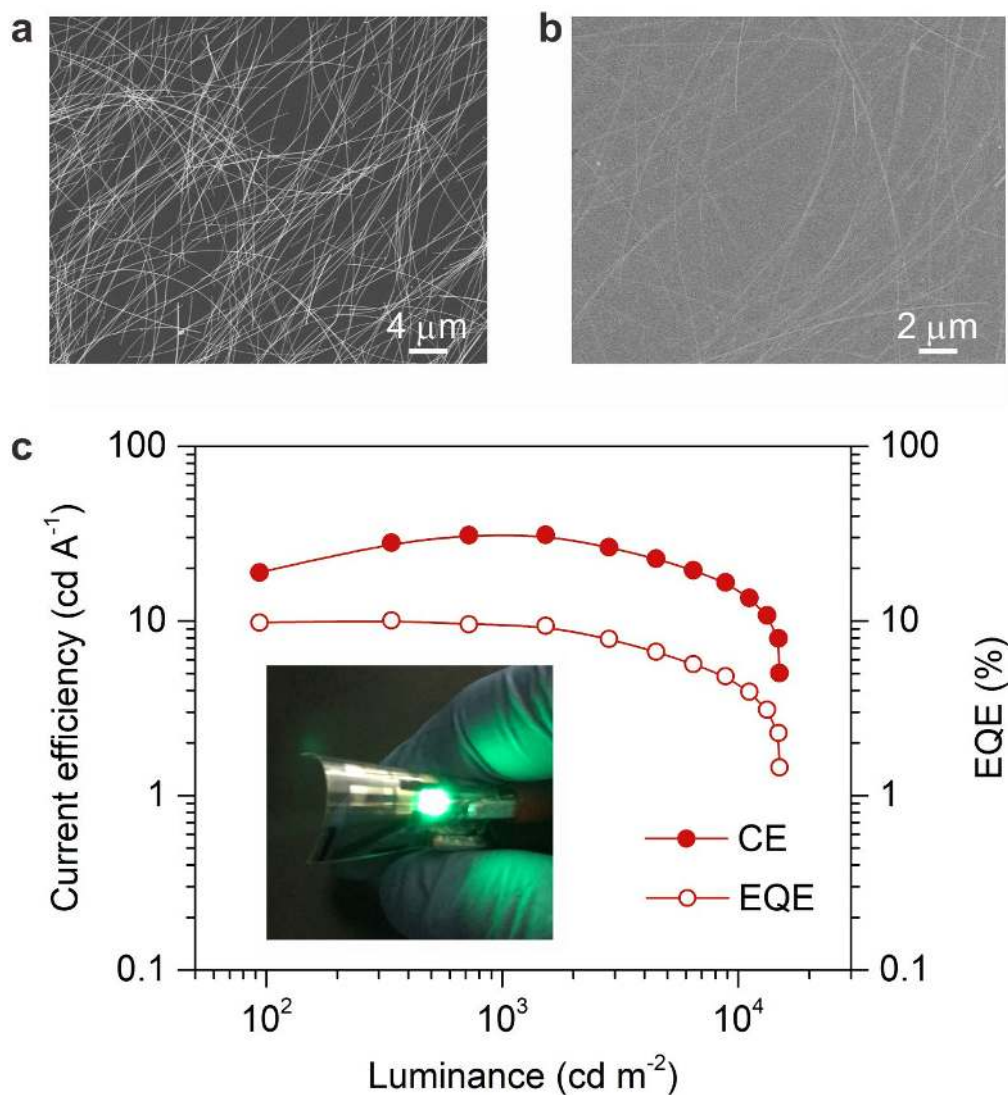
Figure 5. Performance of flexible PeLED on AgNWs-coated PET substrate. (a,b) SEM images of (a) AgNWs electrode on PET substrate and (b) $CsPbBr_3$+PEG+PEABr perovskite film on PEDOT:PSS/AgNWs/PETe. (c) CE and EQE as a function of luminance. Inset: photograph of a flexible device in operation.

Table 1. Performance of CsPbBr$_3$ PeLEDs without and with PEG and PEABr additives.

CsPbBr$_3$ emitter	PL/EL peak [nm]	Max. L [cd m^{-2}]	EQE [%]	CE [cd A^{-1}]	CIE [x, y]
pure	520/518	9662	0.76	2.50	[0.096, 0.750]
PEG	520/520	4161	1.39	5.05	[0.124, 0.783]
PEABr	512/512	11430	2.89	8.09	[0.072, 0.700]
PEG+PEABr	514/514	45990	13.14	37.14	[0.092, 0.753]